Chapter 4

Two-Photon Glutamate Uncaging to Study Structural and Functional Plasticity of Dendritic Spines

Ivar S. Stein, Travis C. Hill, Won Chan Oh, Laxmi K. Parajuli, and Karen Zito

Abstract

The activity-dependent structural remodeling of dendritic spines in response to sensory experience is vital for the dynamic regulation of neuronal circuit connectivity that supports complex behavior. Here, we discuss how the two-photon glutamate uncaging technique can be applied to study the mechanisms that drive activity-dependent structural and functional plasticity in individual dendritic spines. Our goal is to provide the reader with the key background for this technique and to present guidelines, practical details, and potential caveats associated with its implementation.

Key words Glutamate uncaging, Two-photon imaging, Dendritic spine, Synaptic plasticity, Glutamate receptor

1 Introduction

Experience- and activity-dependent modification of the number and strength of synaptic connections drives the refinement of neuronal circuits during learning. Most of the excitatory synapses in the mammalian cerebral cortex occur on dendritic spines, microscopic membranous protrusions from neuronal dendrites [1, 2]. Precise regulation of the growth, stabilization, and elimination of dendritic spines is necessary for learning [3–5]. Spine volume is also dynamically regulated and highly correlated with the number of AMPA-type glutamate receptors (AMPARs), which mediate fast excitatory synaptic transmission; thus, spine size is tightly linked to synaptic function [6]. Indeed, increased synaptic strength through the induction of long-term potentiation (LTP) is associated with spine enlargement [7, 8], while decreased synaptic strength via the induction of long-term depression (LTD) is associated with spine shrinkage or loss [8, 9]. Dysregulation of spine development and plasticity mechanisms can lead to alterations in dendritic spine

morphologies and densities and is associated with cognitive impairments [10]. Thus, study of the mechanisms that regulate spine morphogenesis and stability is critically important for understanding the cellular basis of learning and also how these mechanisms are disrupted in disease.

In this chapter, we describe how photolysis of caged glutamate using two-photon excitation can be implemented to study the mechanisms that drive the structural and functional plasticity of dendritic spines. The development of caged neurotransmitters with adequate two-photon cross sections has revolutionized our ability to study and manipulate single synapses. Stimulation of individual synapses with light-induced neurotransmitter release offers many advantages over traditional electrophysiological approaches. First, light can be delivered with exceptional spatial precision and can be rapidly redirected to stimulate different locations, enabling precise spatiotemporal control compared to stimulation with microelectrodes or perfusion with pharmacological agents. Second, light can be delivered to synapses deep in tissue relatively noninvasively, as compared to electrode placement. Third, unlike electrical stimulation of afferent fibers, uncaging allows the stimulation of single synapses with a single neurotransmitter, permitting study of the effects of that specific neurotransmitter. Fourth, uncaging stimulation bypasses the presynaptic terminal and thus permits investigation of the effect of pharmacological manipulations exclusively on postsynaptic transmission and plasticity mechanisms. Finally, two-photon glutamate uncaging can be combined with calcium imaging and electrophysiological recording to study the functional properties of single synapses. Altogether, two-photon glutamate uncaging provides tremendous advantages for the study of single synapse structural and functional plasticity mechanisms.

1.1 Caged Neurotransmitters

Caged compounds are defined as biologically active molecules that have been rendered inert through chemical modification with a photolabile protecting group. Photostimulation with the appropriate wavelength and intensity of light breaks the covalent bond connecting the protective group, thereby "uncaging" and releasing the active biomolecule. The first successful applications of caged compounds involved the addition of ortho-nitrobenzyl (NB) protecting groups to ATP [11] and cAMP [12], which paved the way for the development of other NB-caged compounds, including neurotransmitters like glutamate [13–15]. However, NB photochemistry is not suitable for two-photon uncaging due to poor two-photon absorption cross section [16]. In this chapter, we focus specifically on the caged glutamates available for studying structural and functional plasticity of dendritic spine synapses. Many different caging strategies and syntheses have been used to produce caged glutamate which can be used with two-photon

Table 1
Properties of caged glutamate compounds suitable for two-photon uncaging

Cage	1P λ_{max} (nm)	Quantum Yield (QY)	Extinction coefficient (ε, M^{-1} cm^{-1})	$\varepsilon \times$ QY	2P λ_{max} (nm)	Rate (s^{-1})	2P action cross section (GM)	Commercially available
MNI-Glu	340	0.08	4500	383	730	10^5	0.06	Yes
CDNI-Glu	330	0.50	6400	3200	720	ND	0.06	No
MDNI-Glu	350	0.47	8600	4042	730	ND	0.06	Yes
RuBi-Glu	450	0.13	5600	728	800	>10^5	0.14	Yes
DEAC450-Glu	450	0.39	43,000	16,800	900	ND	0.50	No
PMNB-Glu	317	0.10	9900	990	800	ND	0.45	No
PENB-Glu	317	0.10	9900	990	740	ND	3.20	No

Abbreviations: *1P* one-photon, λ_{max} absorption maximum, *2P* two-photon, *ND* not determined
The properties of MNI-Glu [6], CDNI-Glu [17], MDNI-Glu [18, 19], RuBi-Glu [20], DEAC450-Glu [21], PMNB-Glu [22], and PENB-Glu [23] have been described. Suppliers of the commercially available glutamate uncaging reagents include, e.g., Tocris, Hello Bio, and Femtonics

excitation, including nitroindoline (NI) derivatives, coumarin derivatives, and novel inorganic compounds, such as ruthenium-bipyridine (RuBi) (Table 1) [6, 17, 20, 21, 24].

In order to be experimentally useful, caged compounds must exhibit several fundamental properties. Most importantly, photorelease or "uncaging" should be efficient in response to the uncaging light and must rapidly lead to the production of the biologically active molecule. The efficiency of photorelease depends on (1) the *extinction coefficient of a molecule*, or how well the caged compound absorbs light, (2) the *quantum yield*, or how often light absorption will lead to photorelease, and (3) the *rate at which light absorption leads to photorelease*. The overall quality of the caged compound is often assessed using the product of the extinction coefficient and the quantum yield at a particular wavelength, which reflects both the efficiency of light absorption and the probability that light absorption will result in successful photorelease.

To best mimic synaptic glutamate release, the rate of photorelease of active glutamate must be considerably faster than the rise time of synaptic glutamate receptor currents. AMPARs are responsible for the fast component of excitatory synaptic currents, which display rise times of 100–500 μs. Photorelease of 4-methoxy-7-nitroindolinyl (MNI)-glutamate occurs within 10 μs, and therefore uncaging of MNI-glutamate can be used to mimic glutamate release and to study excitatory postsynaptic currents [6]. The two-photon action cross section of MNI-glutamate is adequate at 0.06

GM (Göppert-Mayer unit, 1 GM = 10^{-50} cm^4 s/photon) at 730 nm [6]; however, it is ~1000-fold less efficient than its absorption of near-UV light, requiring the use of much higher concentrations of caged reagent (mM) and higher intensity light for successful two-photon uncaging [6, 25].

The successful biological application of caged neurotransmitters also requires *chemical stability* (no hydrolysis at physiological pH and temperature) and *biological inertness* of both the caged compound and the released photolabile protecting group. No hydrolysis of MNI-glutamate can be detected after 8 h at room temperature (pH 7.4) [26] and MNI-caged glutamate has been shown to be inert with no activation of glutamate receptors at concentrations up to 10 mM [6]. Surprisingly (and disappointingly), MNI-glutamate is not biologically inert in that it is a strong antagonist of GABA$_A$ receptors (GABA$_A$Rs) at concentrations commonly utilized for two-photon uncaging [20, 21, 25, 27, 28]. Thus, in the absence of tetrodotoxin (TTX) to block action potentials, bathing a cultured slice in MNI-glutamate can lead to epileptiform-like activity, which can cause problems for cellular and circuit level studies. This antagonistic GABA$_A$R side effect appears to be less dramatic, but still an issue with the more recently developed caged glutamate compounds CDNI-, RuBi-, and DEAC450- (a 7-diethylaminocoumarin derivative) glutamate [17, 20, 21], which are reported to have better two-photon action cross sections and higher extinction coefficients compared to MNI-glutamate (Table 1) and therefore can be used at lower concentrations, reducing the antagonism of GABA$_A$Rs.

Of the caged glutamates with adequate two-photon cross sections (Table 1), MNI-glutamate has been commercially available for the longest time and is well-studied and chemically stable, making it the most widely applied caged glutamate for two-photon uncaging (**see Note 1**). MNI- and CDNI-glutamate have two-photon absorption maxima at 720 nm, whereas RuBi-glutamate and DEAC450-glutamate are red-shifted. The two-photon absorption maximum for RuBi-glutamate is at 800 nm, which is close to the peak of the maximum power output of the Ti:sapphire lasers and therefore could be advantageous when splitting the uncaging beam with a spatial light modulator (SLM) [29, 30]. However, this wavelength is also closer to the wavelengths often used for simultaneous calcium imaging, and therefore care must be taken that the caged compound is not uncaged during imaging. DEAC450-glutamate is even further red-shifted with maximum two-photon photolysis at 900 nm [21]. Thus, DEAC450-caged compounds can be used in combination with other nitroindolinyl-cages like MNI or CDNI, which have their excitation peaks at 720 nm, for two-color, two-photon uncaging. Indeed, another coumarin derivative named N-DCAC-GABA already has been used in combination with CDNI-glutamate for simultaneous two-photon uncaging of glutamate and GABA to

study how excitatory and inhibitory inputs shape dendritic integration [31]. Additional caged glutamate compounds suitable for two-photon uncaging that have been less widely tested include 3-(2-propyl)-4′-methoxy-4-nitrobiphenyl (PMNB)-glutamate and 3-(2-propyl-1-ol)-4′-tris-ethoxy(methoxy)-4-nitrobiphenyl (PENB)-glutamate (Table 1) [22, 23].

1.1.1   Applications of Two-Photon Glutamate Uncaging in the Study of Dendritic Spines

The development of caged compounds suitable for two-photon glutamate uncaging opened the door for the detailed study of synaptic plasticity mechanisms at the single spine level. Uncaging of MNI-glutamate was first used to map how the functional properties of individual spines relate to their structural properties and to demonstrate that spine volume is tightly correlated with the amplitude of excitatory postsynaptic current [6]. Matsuzaki and colleagues further pioneered studies on the structural plasticity of individual dendritic spines, showing that repetitive glutamate uncaging (usually at 0.5–2 Hz) under nominally Mg^{2+}-free conditions, or when coupled with postsynaptic depolarization to 0 mV, induces a rapid and selective enlargement of the stimulated spine, a single-spine structural long-term potentiation (sLTP) [7].

Several groups, including our own, have implemented two-photon glutamate uncaging to study in detail the structural and functional plasticity of spiny synapses. An initial study characterized the functional development of nascent dendritic spines. Notably, new spines expressed glutamate-evoked currents that were indistinguishable from those of mature spines of comparable size, demonstrating that the formation and growth of new spines is tightly coupled to formation and strengthening of glutamatergic synapses [32]. A subsequent study went on to show that these newly formed spines are stabilized long-term by high-frequency glutamate uncaging leading to the induction of LTP of synaptic transmission (Fig. 1a–d) [33]. In contrast, prolonged low-frequency (0.1 Hz) uncaging of glutamate at single spines resulted in spine shrinkage and synaptic depression (Fig. 1e–g) [34]. Intriguingly, NMDA-type glutamate receptor (NMDAR) activation can drive spine shrinkage in the absence of NMDAR-dependent ion flow and Ca^{2+} influx (Fig. 1h–l) [35]. Furthermore, a strong, high-frequency (5 Hz) glutamate uncaging stimulus can also drive the de novo growth of spines from the dendrite (Fig. 1m) [36–38]. These studies give a taste of how simultaneous two-photon imaging and glutamate uncaging can be used in combination with calcium imaging and electrophysiological recordings to study the synaptic plasticity mechanisms at single synapses that underlie learning.

This chapter provides detailed methods on how two-photon imaging can be combined with two-photon glutamate uncaging to
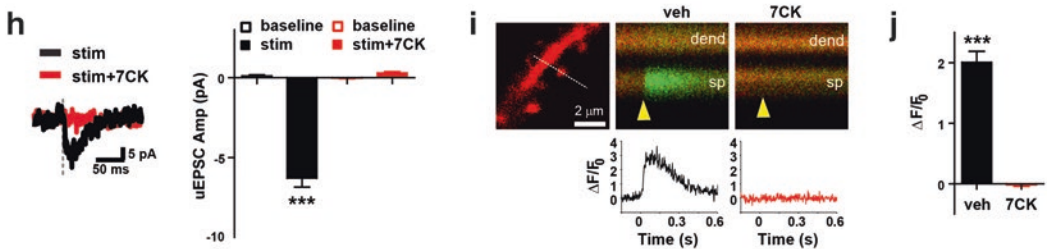
I. High-Frequency Uncaging (HFU) of glutamate increases uEPSC amplitude and size of new spines
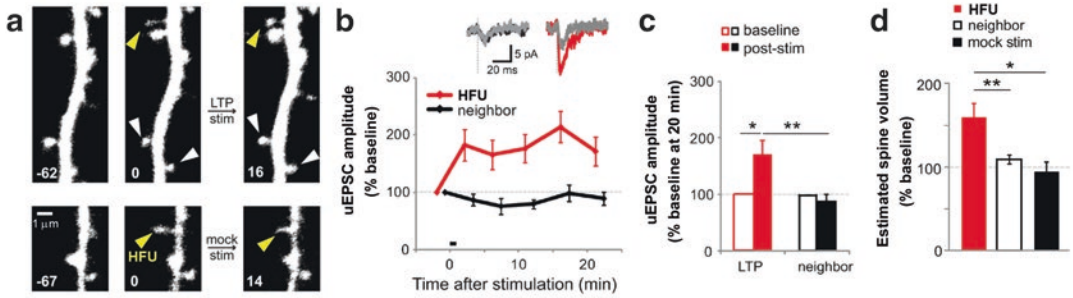
II. Low-Frequency Uncaging (LFU) of glutamate leads to synaptic depression and spine shrinkage
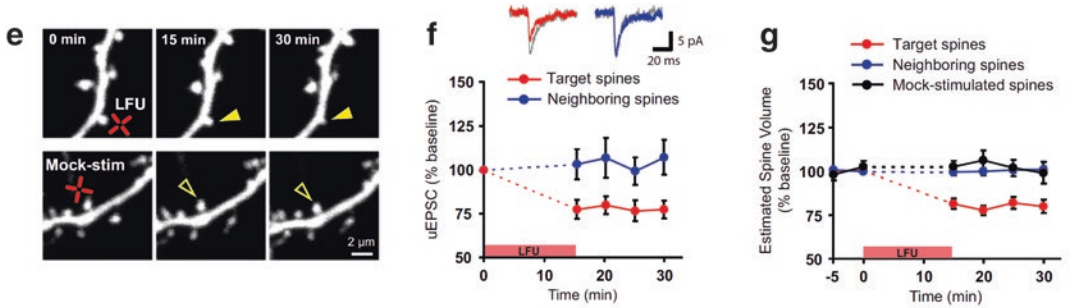
III. Block of ion flow through the NMDAR converts uncaging-induced spine enlargement into shrinkage
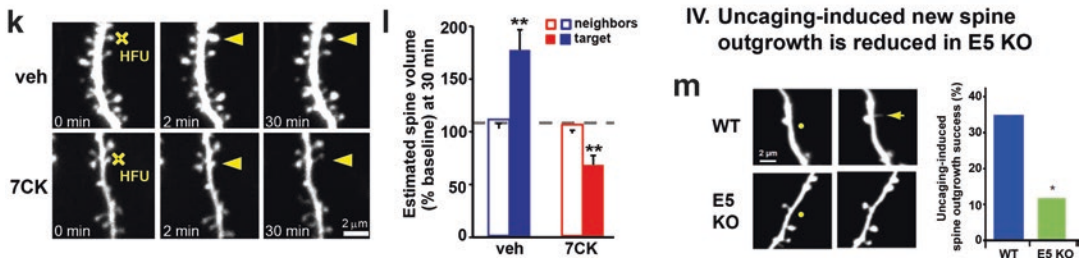

Fig. 1 Examples of plasticity induced by two-photon glutamate uncaging. (**a**) New spines (yellow arrowhead), but not neighbors, enlarge following high-frequency glutamate uncaging (HFU). (**b**, **c**) HFU leads to an increase in the uEPSC of the stimulated spine (red), but not of neighboring spines (black). (**d**) Mock stimulation (black) in the absence of MNI-glutamate does not induce spine growth. (**e**) Target spines shrink following low-frequency uncaging (LFU), but not following mock stimulation (red crosses). LFU but not mock stimulation leads to a decrease in uEPSC amplitude (**f**) and size (**g**) of target spines (red circles), but not unstimulated neighbors (blue circles). (**h**) NMDAR uEPSCs (black) are blocked

study the mechanisms that drive structural plasticity of dendritic spines on pyramidal neurons of the hippocampus.

2   Materials

2.1   Buffers/ACSF/ Drugs

Simultaneous two-photon imaging and glutamate uncaging experiments are performed in perfusing artificial cerebrospinal fluid (ACSF; in mM: 127 NaCl, 25 NaHCO₃, 1.2 NaH₂PO₄, 2.5 KCl, 25 D-glucose, aerated with 95% O_2/5% CO_2, ~310 mOsm, pH 7.2), typically containing 0 Mg^{2+}, 2 mM Ca^{2+}, 1 μM TTX (to block spontaneous spiking activity) and 2.5 mM MNI-glutamate (Tocris) (**see Notes 1 and 2**). Note that there can be batch-to-batch variations in the efficacy of MNI-glutamate (see Methods Sect. 3.6.1).

2.2   Two-Photon Microscope Setup

Figure 2a shows a typical layout of a two-photon microscope for simultaneous imaging and photolysis of caged compounds. For two-photon imaging, power of the infrared (IR) laser (mode-locked Ti:sapphire laser; e.g., Coherent [Santa Clara, CA] or Spectra-Physics [Mountain View, CA]) beam is controlled with a Pockels Cell (e.g., Model 350-80, Conoptics [Danbury, CT]), and xy position is controlled with galvanometers (e.g., Model 6210H, Cambridge Technology [Lexington, MA]). The beam is directed through a scan lens into a conventional upright microscope (e.g., Olympus [Tokyo, Japan]) and through a tube lens and a water-immersion objective designed to readily transmit IR light. To maximize detection of emitted photons, which originate almost exclusively from the focal volume, photomultiplier tubes (PMTs; e.g., R3896, Hamamatsu Photonics [Hamamatsu City, Japan]) both above and below the sample are used and the signals are summed electronically. A second pulsed IR laser beam for uncaging photostimulation is combined with the first beam using a polarizing beam-splitting cube (Thorlabs) and scanned either simultaneously with the imaging beam (Fig. 2a) or independently using a second set of scan mirrors. Alignment of the imaging and

---

Fig. 1 (Continued) by 7-chlorokynurenic acid (7CK, red). (**i**) Image of a dendritic segment from a cell transfected with a red cell fill (DsRedExpress) and the Ca^{2+} indicator GCaMP6 (green). Overlays of red and green fluorescence line-scan images of the target spines (sp) and dendrite (dend) from the region indicated by the white dashed line in the absence or presence of 7CK before and after glutamate uncaging (yellow arrowhead). (**i, j**) NMDAR Ca^{2+} transients (black) are completely blocked by 7CK (red). (**k**, **l**) HFU (yellow crosses) in the presence of 7CK (red) results in shrinkage of the target spine instead of enlargement as seen in vehicle conditions (blue). (**m**) A new spine (yellow arrow) forms following HFU (yellow circle) near a thickened, low-spine density dendritic segment from WT, but not Ephexin 5 (E5) KO mutant mice. The success rate of HFU-induced new spine outgrowth is higher in WT (~35%) than in E5 KO (10%). Panels (**a–d**) are adapted from Hill and Zito (2013) [33] with permission from the Society for Neuroscience. Panels (**e–g**) are adapted from Oh et al. (2013) with permission from the National Academy of Sciences [34] and panels (**h–l**) are adapted from Stein et al. (2015) [35] with permission from the Society for Neuroscience. Panel (**m**) is adapted from Hamilton et al. (2017) [36] with permission from Elsevier
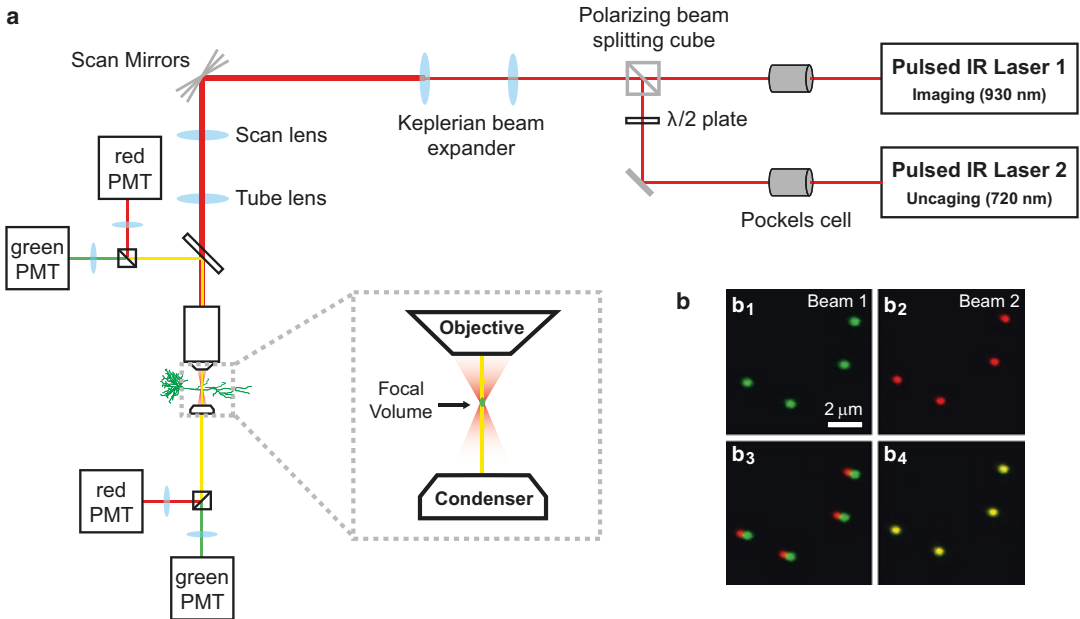
Fig. 2 Microscope setup for simultaneous two-photon imaging and glutamate uncaging. (**a**) For two-photon imaging, the power of the pulsed IR laser is controlled via a Pockels cell and the x-y position is controlled using scan mirrors. Two-photon excitation is restricted to the focal volume (gray inset) and because of this localization of excitation, all emitted photons contribute to the signal and can be collected. Top and bottom PMTs are used to maximize photon collection and the signals are summed electronically. A second pulsed IR laser is used for glutamate uncaging. In this schematic, both the imaging and the uncaging laser beams are controlled by the same set of scan mirrors, but for faster and independent control of the uncaging stimulus the laser beams also can be controlled by two independent sets of scan mirrors and only combined downstream. (**b**) Pseudocolored images of 0.2 μm red fluorescent beads excited with the imaging (b_1, green) or photostimulation (b_2, red) lasers. If the overlay of the bead images shows little overlap (b_3), the angular steering mirrors can be adjusted to bring the two beams in alignment and achieve complete overlap (yellow) of the pseudocolored bead images (b_4)

photostimulation lasers should be regularly monitored and optimized (see Methods Sect. 3.4).

2.3 Software

Data acquisition software needs to be versatile in order to accommodate changes in rig configuration and experimental design. A highly configurable software suitable for two-photon imaging and photostimulation experiments is the open-source software ScanImage and Ephus (http://openwiki.janelia.org/wiki/display/ephus/; [39]; now developed and supported by Vidrio Technologies, LLC), written in MATLAB (The Mathworks [Natick, MA]).

2.4 Electro physiology

Confirming the efficacy of caged neurotransmitters can be accomplished using simultaneous imaging and electrophysiology. Setting up electrophysiology on a two-photon microscope is relatively straightforward. At minimum, the setup consists of an amplifier, a

head stage, recording and ground electrodes, micromanipulators, shielding, and a perfusion system. There are a few special considerations when setting up for simultaneous electrophysiology and two-photon microscopy. First, because two-photon imaging experiments are typically performed in vivo or in deep tissue of brain slices, the microscope should be upright (not inverted) and should have a water-immersion objective with a long working distance (providing space for the microelectrodes to access the specimen). We use an Olympus LUMPLFL60×/W, which has a numerical aperture (NA) of 1.0 and a working distance of 2 mm. Second, stepper motors and preamplifiers can be considerable sources of electrical noise, so care should be taken to properly ground these items. Third, shutters can be a considerable source of vibrational noise; anchoring shutters to the optical table using nylon screws can significantly diminish this noise. Finally, it is important to plan ahead so that recording pipettes are positioned in a way that does not interfere with image acquisition and, when using dye-filled pipettes, imaging regions should be distant from the pipette and dye spill should be minimized by approaching the cell quickly and reducing the positive pressure applied to the pipette because excessive dye spill confounds image analysis [40].

3   Methods

3.1   Preparation and Transfection of Organotypic Hippocampal Slice Cultures

Preparation of organotypic hippocampal slice cultures from postnatal day 6–8 (P6-8) rodent brain according to the interface method [41] has been described [42–44]. Biolistic transfection of rat hippocampal slices cultures has been described in detail elsewhere [45].

3.2   Preparation of Acute Hippocampal Slices

Acute slice preparation protocols will vary depending upon species, age, and brain area. Acute hippocampal slice preparation from P16-19 rodents has been described [46, 47]. Acute slices can be prepared from transgenic mice with sparsely labeled neurons, such as Thy-1-GFP-M [48], or from animals that have been transfected using in utero electroporation [49, 50] or transduced by injection with low titers of virus [51]. Alternatively, individual cells from wild-type (WT) slices can be loaded with dyes or calcium indicators by diffusion from patch pipettes [52, 53].

3.3   Two-Photon Time-Lapse Imaging

When imaging the morphology of fluorescently labeled neurons in brain tissue, two-photon microscopy provides distinct advantages due to reduced background fluorescence and decreased phototoxicity compared to wide-field and confocal microscopy [54].

Step-by-Step Instructions:

1. Screen for fluorescently labeled CA1 pyramidal neurons using a dissecting stereomicroscope with fluorescence or an epifluorescence microscope with a 10× air objective. Note that following biolistic transfection, incubate 1–2 days for expression of small cytosolic proteins, such as Enhanced Green Fluorescent Protein (EGFP), and 3–4 days for expression of large or membrane-bound proteins. Viral expression typically takes 1–2 weeks.

2. Place organotypic or acute hippocampal slices in an imaging chamber perfused with recirculating ACSF with custom concentrations of Mg^{2+} and Ca^{2+}. For uncaging spine plasticity experiments, the ACSF often contains nominally 0 Mg^{2+}, 2 mM Ca^{2+}, 0.001 mM TTX, and 2.5 mM MNI-glutamate (**see Notes 1 and 2**) and is maintained at 30 °C (e.g., heater Model TC-324B, Warner Instruments). Organotypic slices can be held in place with a horseshoe of inert gold wire (Alfa Aesar # 10966-BQ), which is placed to weigh down the attached piece of membrane from the cell culture insert (Millipore # PICM0RG50). Acute slices can be held in place with a harp (Warner Instruments # 64-1421).

3. Neurons situated in a healthy (**see Note 3**) cell layer typically at depths of 20–50 μm are imaged using a custom two-photon microscope with a pulsed Ti:sapphire laser tuned to 930 nm, which excites GFP and most red fluorophores, simultaneously. To avoid bleaching and phototoxicity, use imaging powers in the range of 0.5–2 mW at the sample (hand-held power meter, e.g., Coherent # 1098293).

4. For each neuron, image stacks (512 × 512 pixels; ~0.02–0.04 μm per pixel) with 1 μm z-steps (typically 10–15 slices) are collected from secondary or tertiary apical or basal dendrites, 40–100 μm from the soma. Each dendritic segment is repeatedly imaged at defined intervals (e.g., every 5 min). Typically, at least two baseline images are taken before glutamate uncaging, and then the dendritic segments are followed for at least 30 min following uncaging stimulation.

3.4 Beam Alignment   Precise alignment of the imaging and uncaging lasers is essential for accurate and successful single spine stimulation. Laser alignment can be checked using subresolution 0.1 or 0.2 μm fluorescent beads (e.g., F8810, F8803, Thermo Fisher Scientific), which can be alternately excited using either the imaging or uncaging laser (Fig. 2b). If the beams are not in perfect alignment, the overlay of the bead images will not overlap completely, and the angular steering mirrors should be adjusted until the two beams are in alignment in xy and there is complete overlap of the bead images excited with the two different lasers. Because the resolution limit in the z-axis is ~2 μm, the slight offset of the uncaging (720 nm)

and imaging (930 nm) beams in z-axis due to the different focal points of the distinct wavelengths is typically not of concern.

3.5 Photostimulation   Photostimulation can be accomplished either during scanning or by parking of the uncaging laser beam at a single spot. Photostimulation during scanning allows for simultaneous imaging and real time monitoring of the uncaging beam localization but has the disadvantage that the stimulation time and frequency are constrained by the field of view. Consequently, this configuration usually requires shorter stimulation times and higher laser powers. Beam parking, on the other hand, has the advantage of flexible stimulation times and frequencies but, when used on setups with only one set of scan mirrors, is associated with a slight delay before imaging and does not allow real time monitoring of the uncaging beam or sample drift. The accuracy of photostimulation during beam parking with one set of scan mirrors can be tested by bleaching of fluorescent beads (Fig. 3a–d) or bleaching of specific patterns in a fluorescent slide (e.g., 2273, Ted Pella; Fig. 3e, f).
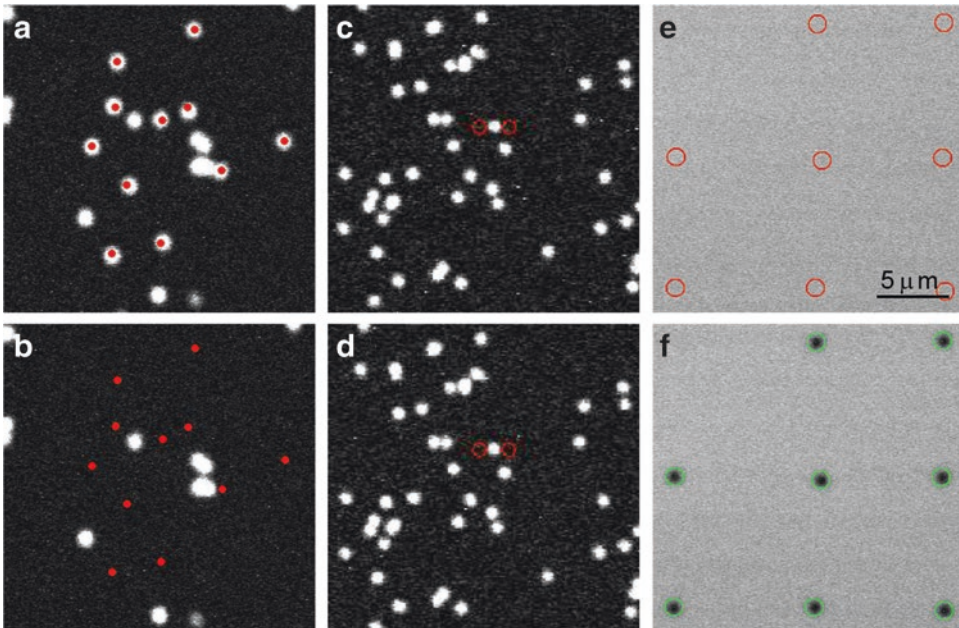

Fig. 3 Testing the accuracy of beam parking for photostimulation. Images of subresolution 0.2 μm red fluorescent beads before (**a**) and after (**b**) photobleaching of a selected subset of the beads (red dots). Due to the localization of excitation of two-photon imaging, targeting of the photostimulation directly next to the fluorescent beads (red circles, **c**), instead of directly on them (**a**, red dots), does not lead to bleaching (**d**). (**e**) Image of a fluorescent slide on which the beam parking targets were defined (red circles) and selectively bleached, indicated as loss of fluorescence signal in the green circles (**f**)

3.6 Glutamate Uncaging to Study the Structural and Functional Plasticity of Dendritic Spines

Two-photon uncaging of MNI-glutamate is achieved through irradiation with a pulse (0.25–4 ms) of 720 nm light from a mode-locked Ti:sapphire laser. The power used to uncage MNI-glutamate will depend on the pulse duration, the depth of the target in the tissue, the concentration of MNI-glutamate in the bath, and the numerical aperture of the objective. The duration and power of the uncaging stimulus can be adjusted so that the kinetics of the uncaging-evoked Excitatory PostSynaptic Currents (uEPSCs) closely mimic those of miniature excitatory postsynaptic currents (mEPSCs) [6]. The spatial resolution of two-photon uncaging permits stimulation of individual dendritic spines [6].

3.6.1 Calibration of the Glutamate Uncaging Stimulus

To calibrate the glutamate uncaging stimulus, visually identified CA1 pyramidal neurons in slice culture (DIV14–18, depths of 20–50 μm) are patched (pipette tip resistances, 5–7 MΩ) in whole-cell configuration (V_{hold} = −65 mV; series resistances, 15–45 MΩ) using Cs-based internal solution (in mM: 135 Cs-methanesulfonate, 10 HEPES, 10 Na_2 phosphocreatine, 4 $MgCl_2$, 4 Na_2-ATP, 0.4 Na-GTP, 3 Na L-ascorbate, and 0.2 Alexa Fluor 488, and ~300 mOsm, pH ~7.25) in standard ACSF containing 2 mM Ca^{2+}, 1 mM Mg^{2+}, 1 μM TTX, and 2.5 mM MNI-glutamate at 25 °C. uEPSCs are evoked using 1 ms laser pulses (720 nm) at the power to be tested (typically around 10 mW at the sample) at five spines per cell within 50 μm of the soma on secondary and tertiary apical and basal dendrites (Fig. 4a). Data acquisition is managed with open-source Ephus software (http://openwiki.janelia.org/wiki/display/ephus/; [55]).

uEPSC amplitudes from individual spines are quantified as the average (5–7 test pulses at 0.1 Hz) from a 2 ms window centered on the maximum current amplitude within 50 ms following pulse delivery. The average uEPSC amplitudes of these 5–7 test pulses should be robust and stable, although individual responses to each single photostimulation are variable (Fig. 4b). Uncaging pulse power should be adjusted with each individual batch of MNI-glutamate to elicit equivalent responses. We aim for an average amplitude of ~10 pA recorded at the soma (at a concentration of 2.5 mM MNI-glutamate and pulse duration of 1 ms) (Fig. 4c), which mimics the amplitude of a quantal response measured at moderate to large synapses [56]. To guarantee stable and comparable uEPSC amplitudes, choose a test pulse frequency that does not lead to changes in the uEPSC amplitude with time (Fig. 4d, e). In addition, the stimulated spine should be greater than 1 μm away from neighboring spines to minimize activation of nearby spines due to glutamate spillover.

It is helpful if the software used for extended time-lapse imaging and glutamate uncaging incorporates a mechanism to correct for drift. In our customized ScanImage software, lateral drift is determined by acquisition of an image immediately before the uncaging stimulation and calculating the cross correlation with an
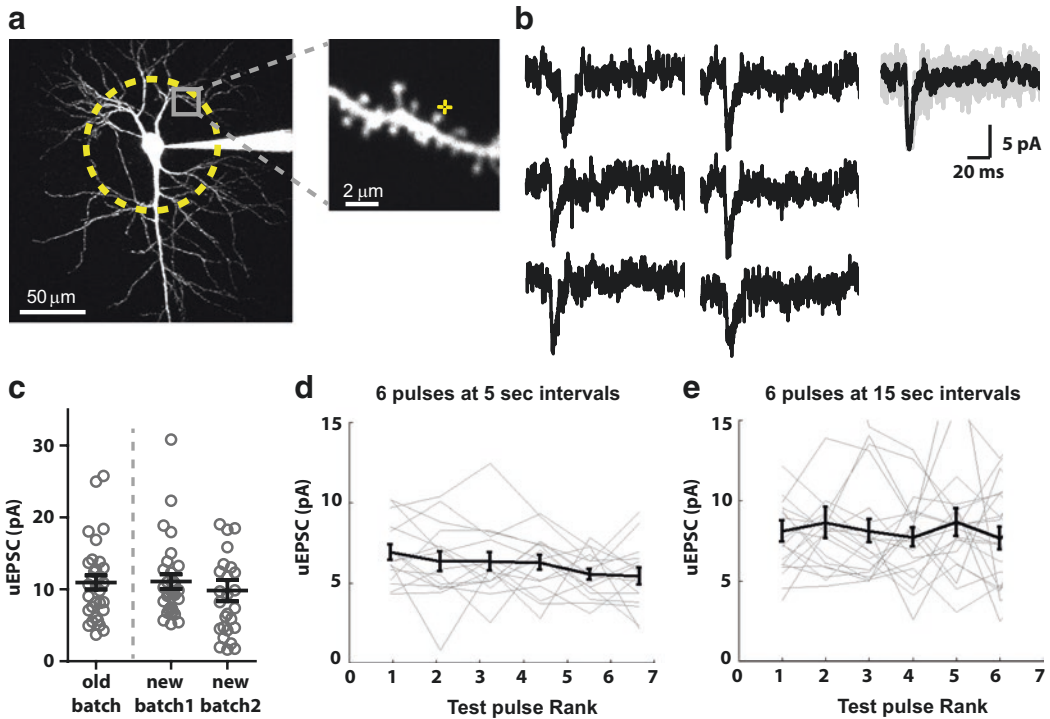
Fig. 4 Testing of individual MNI-glutamate batches. (**a**) Image of a CA1 pyramidal cell filled with Alexa 488 through the recording electrode. Spines are stimulated within a 50 μm radius from the cell body (illustrated as dashed yellow line). Inset shows a dendritic segment with the stimulated spine (yellow cross). (**b**) Individual uEPSC traces evoked by six subsequent uncaging pulses on the same spine (black) and the representative average uEPSC (black) with the six individual responses (gray). (**c**) The average AMPAR uEPSC amplitudes (mean ± SEM) between the old and two new tested batches of MNI-glutamate show no difference between the old and first new batch of glutamate. The second new tested batch of MNI-glutamate has a slightly reduced average AMPAR uEPSC amplitude, which could be adjusted by increasing the power of the uncaging laser pulse. (**d**) Delivery of uncaging test pulses at 5 s intervals on the same spine leads to a reduction of the average uEPSC amplitude (black) over time. (**e**) Increasing the test pulse interval to 15 s results in a stable average uEPSC amplitude (black) over time

initial reference image from the same time series. The drift is then automatically corrected by adjustment of the galvanometer scanning angles (Fig. 5).

The calibration of the MNI-glutamate batch is based on averaging the responses of multiple spines on multiple cells at varying depths in the tissue. It is important to note that, even if the laser power at the objective is held constant, the laser power delivered to the target spine will vary depending on the depth of the target spine in the brain slice and the properties of the tissue above the dendritic region of interest (ROI), which influence how much of the excitation light is scattered and absorbed. Inhomogeneous refraction indices due to tissue structure can affect the degree and volume over which the delivered power is spread. Because it is
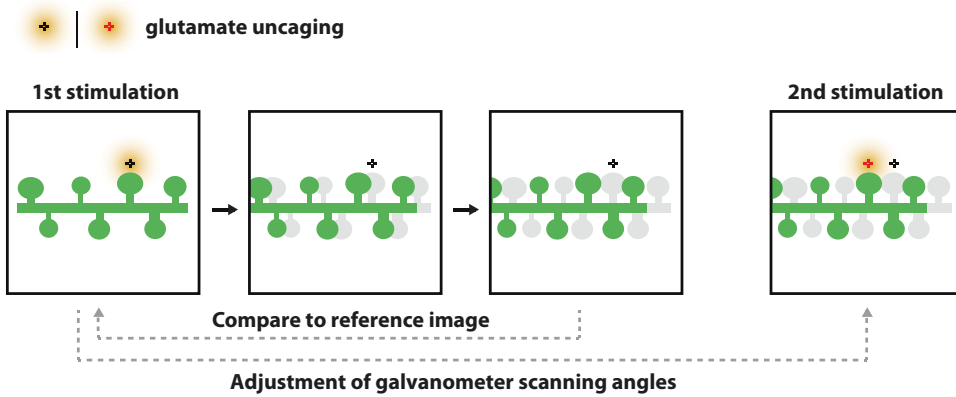
Fig. 5 Drift correction by cross-correlation. Our image acquisition and uncaging software is designed to automatically collect a frame scan image immediately before every uncaging stimulation, and the cross-correlation of this image (green) with a reference image (gray) is used to calculate lateral drift, which is automatically corrected by adjustment of the galvanometer scanning angles so that the uncaging spot (black cross) is redirected to the target spine (red cross)

usually not possible to measure these differences in optical properties of individual brain slices, we typically limit ourselves to a depth range of 20–40 μm and operate under the assumption that variations will average out across multiple cells in different slices from multiple different dissections. Alternatively, others have used a photobleaching protocol to calibrate the laser power for each spine of interest by monitoring bleaching fraction and adjusting power to bleach a constant fraction of the fluorescent dye that fills the spine [57]. While elegant in design, one caveat with this approach is that direct irradiation of the spine with high laser powers can result in cell damage.

3.6.2 Repetitive Glutamate Uncaging for the Induction of Structural Plasticity

The repetitive two-photon uncaging of MNI-glutamate has been shown to induce both input-specific LTP of synaptic transmission and enlargement of spine size (sLTP) [7, 33, 46, 58]. Repetitive glutamate uncaging, at frequencies of 0.5–2 Hz (30–60 stimuli) under low Mg^{2+} conditions, or when paired with postsynaptic depolarization to 0 mV, induces a robust, long-term enlargement of the stimulated spine head and increase in uncaging-evoked spine EPSCs that are stable for at least the next 30 min (Fig. 1a–d, k, l).

In the example illustrated in Fig. 6, the structural plasticity-inducing high-frequency uncaging stimulus consisted of 60 pulses (720 nm, 10 mW at the sample) of 2 ms duration delivered at 2 Hz in 2 mM Ca^{2+}/0 Mg^{2+} ACSF containing 1 μM TTX and 2.5 mM MNI-glutamate ([35, 59] or see similar protocols [7, 33, 46, 60, 61]). During the photostimulation, the uncaging beam (720 nm) is parked at a point ~0.5 μm from the edge of the spine head on the side furthest from the dendrite. Typically, only one dendritic region of interest is stimulated and imaged per cell (*see* **Notes 4 and 5**).
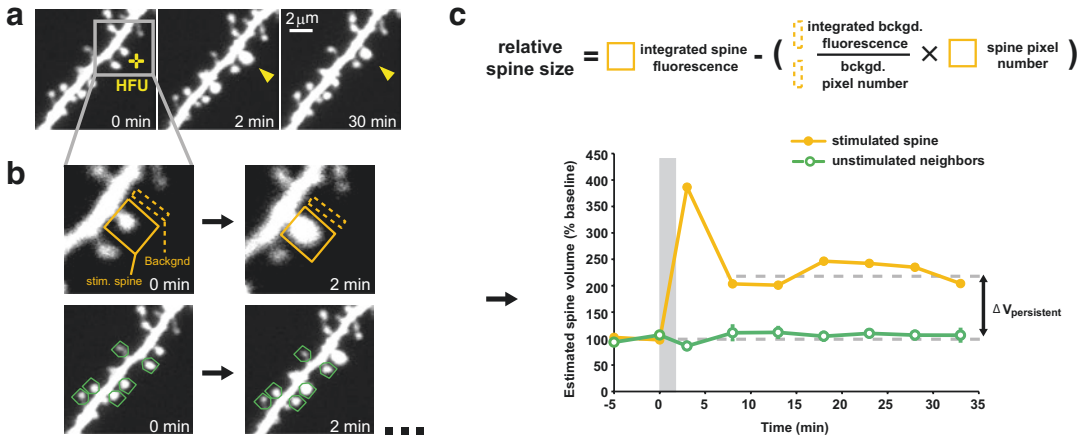
Fig. 6 Analysis of spine size following glutamate uncaging-induced structural plasticity. (**a**) Time-lapse images showing enlargement of the target spine (yellow arrowheads) in response to high-frequency uncaging (HFU, yellow cross) of glutamate. (**b**) 2x magnification of the area around the target spine before (0 min, left) and after (2 min, right) glutamate uncaging. The target region of interest (ROI) drawn around the stimulated spine (solid yellow box) is drawn on the slice in the z-stack in which the analyzed spine is the brightest. A thinner neighboring ROI spanning the same lateral distance from the dendrite (dashed yellow box) is used to measure the fluorescent intensity of the adjacent background. (**c**) The average pixel intensity from the background box is multiplied with the number of pixels of the target ROI to generate the integrated background value, which is subtracted from the integrated pixel intensity of the target spine to calculate the actual fluorescence intensity of the target spine. Graph shows the time course of the estimated volume (normalized to the average of the two baseline images before HFU) of the stimulated spine (yellow) compared to the unstimulated neighbors (green). $\Delta V_{\text{persistent}}$ is the stable increase observed 30 min after HFU

One limitation to consider when studying simultaneous functional and structural plasticity under whole-cell recording conditions is the loss of the ability to induce synaptic plasticity soon after the start of the recording (~5 min) due to the washout (into the recording pipette) of intracellular signaling molecules critical for the induction of plasticity [62, 63]. The rate with which washout influences plasticity induction depends on the recording electrode resistance and the distance of the stimulated spine synapse from the electrode. Washout critically limits the time available for a stable baseline recording before induction of structural and functional plasticity, and in a CA1 pyramidal cell can occur within ~5 min after achieving whole-cell configuration for synapses within 100 μm from the soma. To avoid this washout of intracellular signaling molecules, perforated patch-clamp recordings from neurons transfected with fluorescent proteins can be used [46].

3.7 Quantification of Fluorescence Intensities in Dendritic Spines

Because the size of dendritic spines is often smaller than the resolution limit of the two-photon microscope, spine size and morphology cannot be determined by measuring the apparent spine head diameter. Instead, we use the integrated fluorescence intensity from the spine head as an approximate measure of spine size. Transfection with genetically encoded monomeric and freely diffusible cytoplasmic fluorescent proteins like EGFP highlights cellular morphology and also can be used to assess the relative volume of dendritic spines. Assuming a relatively homogeneous distribution of the fluorescent cell fill, spine brightness should be proportional to the spine volume. Indeed, comparison of fluorescence intensity measurements and subsequent reconstruction with serial section electron microscopy supports that spine brightness is a fairly accurate method for estimating spine volumes [64]. Spine size analysis can be performed using most image analysis software, including ImageJ/Fiji.

Spine brightness or the estimated spine volume is measured from the stimulated target spine and from those neighboring spines that are isolated from other spines and distinguishable from the parent dendrite (laterally projecting from the dendrite in the xy plane) throughout the whole time-lapse imaging series. Due to the lower resolution on the z-axis, spines projecting in the z plane are difficult to distinguish and therefore are not analyzed. Estimated spine volume is measured from background-subtracted green (EGFP) fluorescence images using the integrated pixel intensity of a boxed ROI surrounding the spine head (Fig. 6). The ROIs are drawn in the single z-stack slice in which the analyzed spine is the brightest and the summed pixel intensities (integrated fluorescence intensity) are calculated. To account for the higher background fluorescence in the immediate vicinity of the dendrite, the adjacent background fluorescence is subtracted. Because neighboring spines or other bypassing neurites often prevent placement of the same-sized box adjacent to the target spine, the average pixel intensity of a thinner box spanning the same lateral distance from the dendrite as the target spine box is calculated, multiplied with the pixel number of the target spine box, and subtracted (Fig. 6b, c). The background-subtracted fluorescence intensity is proportional to the spine volume and can be compared to baseline before plasticity induction or to that of unstimulated neighbors (Fig. 6c).

When a new uncaging-induced spine structural plasticity protocol is established, the measured structural changes should be compared to a mock stimulation, which is carried out under identical conditions in the absence of MNI-glutamate [33, 34]. In situations where glutamate spill over is a concern, a laterally shifted stimulation, which releases the same amount of glutamate at a similar distance away from the dendrite without an intervening spine, is an important control [32, 59].

The sample size required to achieve statistical significance depends on the response size and variability that results from the specific structural or functional plasticity paradigm. We average all spines from one cell and then calculate statistics across cells. At minimum, three independent slice culture dissections or acute slice preparations from rodents from both sexes are utilized for each measurement. Image analysis is performed blind to the experimental condition.

Step-by-Step Instructions:

1. Open the images from the time-lapse series and make sure the target spine is clearly identifiable and not obscured by any other structures throughout the whole time-lapse series.

2. Starting with the first time point, identify the image slice in the z-stack in which the target spine is the brightest.

3. Draw a rectangular box around the target spine. Make sure the size of the box can accommodate the changes in spine morphology observed throughout the time-lapse series (*see* **Notes 6 and 7**). Measure the *integrated* fluorescence intensity from this box.

4. Draw a thin box in the neighboring region to the spine box that spans equal distance from the parent dendrite. Due to the high spine densities in mature hippocampal slices, the measurement of a thin background box (as shown in Fig. 6b) is usually preferable, because it will not overlap with neighboring spines or dendritic structures. Measure the *average* fluorescence intensity in this box.

5. To calculate the actual fluorescence intensity of the target spine, background subtraction must be performed. Multiply the average pixel intensity for the thinner background box with the pixel number of the target spine box to calculate the background value, which is now normalized for the difference in size of the background box and can be subtracted from the integrated pixel intensity of the target spine box to give the fluorescence intensity of the target spine (Fig. 6c).

6. Copy the same boxes over to the appropriate image slice in the z-stack from the next time point and repeat the measurements for the remainder of the time-lapse series. For each time point, make sure that the values are measured in the z-stack slice where the target spine is the brightest.

4   Notes

1. Although MNI-glutamate does not spontaneously hydrolyze or photolyze easily, for exposures longer than a few minutes it is wise to keep the main room lights off or to cover the lights with a yellow filter (Rosco #10 filter). These precautions are particu-

larly important for the red-shifted RuBi-glutamate, which is more light-sensitive than MNI-glutamate. For RuBi-glutamate usage, computer screens should be covered with red filters (Rosco #27 filter), absorbing the blue and green wavelengths [20].

2. To minimize the amount of MNI-glutamate used per experiment, ACSF volume is kept low (5–7 ml) and the bath is recirculated using a peristaltic pump (Watson Marlow Sci Q400). Recirculating ACSF is aerated with 95% O_2/5% CO_2, which is first bubbled through a conical tube containing ultrapure water. This additional step allows the humidification of the 95% O_2/5% CO_2 gas mixture before entering the ACSF solution, thus, reducing evaporation and minimizing changes in ACSF osmolarity.

3. Use only intact hippocampal slices with clearly visible dentate gyrus (DG), CA3 and CA1 regions, which are thinned down to 4–8 layers of cells with smooth visible cell somata. Exclude any unhealthy slice cultures and cells. Healthy transfected CA1 pyramidal cells should display fluorescence throughout their dendritic arbor (in case of small, freely diffusible fluorescence molecules) and show no signs of degeneration, with a typical spine density and no signs of dendritic blebbing. Make sure overall spine density does not significantly change during the time-lapse imaging session, because widespread spine elimination or excessive formation of filopodia-like structures can be a sign of compromised cell health.

4. When studying mechanisms of spine growth, choose small spines for studies of spine enlargement and stabilization, as large spines have been reported to show only a transient increase in spine size [7]. For studies on spine shrinkage and elimination, use spines that have been present already for at least one baseline time point during the time-lapse imaging series prior to uncaging stimulation in order to reduce the percentage of transient spines that spontaneously shrink and eliminate in the absence of stimulation.

5. Signaling molecules from the stimulated spine can spread into the parent dendrite over 5–10 μm and therefore, unless the goal is to study cross-talk, it is best to avoid stimulation of a second spine on the same dendritic segment [46, 65, 66]. Note that it also has been reported that the stimulation of three or more spines on dispersed dendritic branches can be sufficient to activate nuclear Erk and thus modify cellular transcription rates [67].

6. When choosing the target spine ROI for analysis of structural plasticity, keep in mind that the spine will grow, so be sure to draw the ROI large enough to include all of the spine even on the final image. Also, pay attention that the ROI is aligned to the spine in all time points, even in the case that the image is drifting.

7. It is not possible to make accurate measurements of stubby spines, which exhibit no detectable spine neck. Without an obvious separation from the dendrite due to the spine neck, the distinction of the spine from the dendrite is arbitrary and fluorescence signals from spine and dendrite will be mixed and inseparable.

Acknowledgments

References

1. Harris KM, Kater SB (1994) Dendritic spines: cellular specializations imparting both stability and flexibility to synaptic function. Annu Rev Neurosci 17:341–371

2. Yuste R, Majewska A, Holthoff K (2000) From form to function: calcium compartmentalization in dendritic spines. Nat Neurosci 3:653–659

3. Hayashi-Takagi A, Yagishita S, Nakamura M et al (2015) Labelling and optical erasure of synaptic memory traces in the motor cortex. Nature 525:333–338

4. Segal M (2017) Dendritic spines: morphological building blocks of memory. Neurobiol Learn Mem 138:3–9

5. Stein IS, Zito K (2018) Dendritic spine elimination: molecular mechanisms and implications. Neuroscientist. https://doi.org/10.1177/1073858418769644

6. Matsuzaki M, Ellis-Davies GC, Nemoto T et al (2001) Dendritic spine geometry is critical for AMPA receptor expression in hippocampal CA1 pyramidal neurons. Nat Neurosci 4:1086–1092

7. Matsuzaki M, Honkura N, Ellis-Davies GC et al (2004) Structural basis of long-term potentiation in single dendritic spines. Nature 429:761–766

8. Okamoto K, Nagai T, Miyawaki A et al (2004) Rapid and persistent modulation of actin dynamics regulates postsynaptic reorganization underlying bidirectional plasticity. Nat Neurosci 7:1104–1112

9. Zhou Q, Homma KJ, Poo MM (2004) Shrinkage of dendritic spines associated with long-term depression of hippocampal synapses. Neuron 44:749–757

10. Penzes P, Cahill ME, Jones KA et al (2011) Dendritic spine pathology in neuropsychiatric disorders. Nat Neurosci 14:285–293

11. Kaplan JH, Forbush B 3rd, Hoffman JF (1978) Rapid photolytic release of adenosine 5′-triphosphate from a protected analogue: utilization by the Na:K pump of human red blood cell ghosts. Biochemistry 17:1929–1935

12. Engels J, Schlaeger EJ (1977) Synthesis, structure, and reactivity of adenosine cyclic 3′,5′-phosphate benzyl triesters. J Med Chem 20:907–911

13. Callaway EM, Katz LC (1993) Photostimulation using caged glutamate reveals functional circuitry in living brain slices. Proc Natl Acad Sci U S A 90:7661–7665

14. Wieboldt R, Gee KR, Niu L et al (1994) Photolabile precursors of glutamate: synthesis, photochemical properties, and activation of glutamate receptors on a microsecond time scale. Proc Natl Acad Sci U S A 91:8752–8756

15. Wilcox M, Viola RW, Johnson KW et al (1990) Synthesis of photolabile precursors of amino acid neurotransmitters. J Org Chem 55:1585–1589

16. Aujard I, Benbrahim C, Gouget M et al (2006) O-nitrobenzyl photolabile protecting groups with red-shifted absorption: syntheses and uncaging cross-sections for one- and two-photon excitation. Chemistry 12:6865–6879

17. Ellis-Davies GC, Matsuzaki M, Paukert M et al (2007) 4-Carboxymethoxy-5,7-dinitroindolinyl-Glu: an improved caged glutamate for expeditious ultraviolet and two-photon photolysis in brain slices. J Neurosci 27:6601–6604

18. Chiovini B, Turi GF, Katona G et al (2014) Dendritic spikes induce ripples in parvalbumin interneurons during hippocampal sharp waves. Neuron 82:908–924

19. Fedoryak OD, Sul JY, Haydon PG et al (2005) Synthesis of a caged glutamate for efficient one- and two-photon photorelease on living cells. Chem Commun (Camb) 29:3664–3666

20. Fino E, Araya R, Peterka DS et al (2009) RuBi-glutamate: two-photon and visible-light photoactivation of neurons and dendritic spines. Front Neural Circuits. https://doi.org/10.3389/neuro.04.002.2009

21. Olson JP, Kwon HB, Takasaki KT et al (2013) Optically selective two-photon uncaging of glutamate at 900 nm. J Am Chem Soc 135:5954–5957

22. Gug S, Charon S, Specht A et al (2008) Photolabile glutamate protecting group with high one- and two-photon uncaging efficiencies. Chembiochem 9:1303–1307

23. Specht A, Bolze F, Donato L et al (2012) The donor-acceptor biphenyl platform: a versatile chromophore for the engineering of highly efficient two-photon sensitive photoremovable protecting groups. Photochem Photobiol Sci 11:578–586

24. Canepari M, Nelson L, Papageorgiou G et al (2001) Photochemical and pharmacological evaluation of 7-nitroindolinyl-and 4-methoxy-7-nitroindolinyl-amino acids as novel, fast caged neurotransmitters. J Neurosci Meth 112:29–42

25. Palma-Cerda F, Auger C, Crawford DJ et al (2012) New caged neurotransmitter analogs selective for glutamate receptor sub-types based on methoxynitroindoline and nitrophenylethoxycarbonyl caging groups. Neuropharmacology 63:624–634

26. Ellis-Davies GC (2007) Caged compounds: photorelease technology for control of cellular chemistry and physiology. Nat Methods 4:619–628

27. Kantevari S, Passlick S, Kwon HB et al (2016) Development of anionically decorated caged neurotransmitters: in vitro comparison of 7-Nitroindolinyl- and 2-(p-Phenyl-o-nitrophenyl)propyl-based photochemical probes. Chembiochem 17:953–961

28. Matsuzaki M, Hayama T, Kasai H et al (2010) Two-photon uncaging of gamma-aminobutyric acid in intact brain tissue. Nat Chem Biol 6:255–257

29. Lutz C, Otis TS, DeSars V et al (2008) Holographic photolysis of caged neurotransmitters. Nat Methods 5:821–827

30. Nikolenko V, Watson BO, Araya R et al (2008) SLM microscopy: scanless two-photon imaging and photostimulation with spatial light modulators. Front Neural Circuits. https://doi.org/10.3389/neuro.04.005.2008

31. Kantevari S, Matsuzaki M, Kanemoto Y et al (2010) Two-color, two-photon uncaging of glutamate and GABA. Nat Methods 7:123–125

32. Zito K, Scheuss V, Knott G et al (2009) Rapid functional maturation of nascent dendritic spines. Neuron 61:247–258

33. Hill TC, Zito K (2013) LTP-induced long-term stabilization of individual nascent dendritic spines. J Neurosci 33:678–686

34. Oh WC, Hill TC, Zito K (2013) Synapse-specific and size-dependent mechanisms of spine structural plasticity accompanying synaptic weakening. Proc Natl Acad Sci U S A 110:E305–E312

35. Stein IS, Gray JA, Zito K (2015) Non-ionotropic NMDA receptor signaling drives activity-induced dendritic spine shrinkage. J Neurosci 35:12303–12308

36. Hamilton AM, Lambert JT, Parajuli LK et al (2017) A dual role for the RhoGEF Ephexin5 in regulation of dendritic spine outgrowth. Mol Cell Neurosci 80:66–74

37. Hamilton AM, Oh WC, Vega-Ramirez H et al (2012) Activity-dependent growth of new dendritic spines is regulated by the proteasome. Neuron 74:1023–1030

38. Kwon HB, Sabatini BL (2011) Glutamate induces de novo growth of functional spines in developing cortex. Nature 474:100–104

39. Pologruto TA, Sabatini BL, Svoboda K (2003) ScanImage: flexible software for operating laser scanning microscopes. Biomed Eng Online 2:13

40. Yasuda R, Nimchinsky EA, Scheuss V et al (2004) Imaging calcium concentration dynamics in small neuronal compartments. Sci STKE 2004:pl5

41. Stoppini L, Buchs PA, Muller D (1991) A simple method for organotypic cultures of nervous tissue. J Neurosci Meth 37:173–182

42. De Simoni A, Yu LM (2006) Preparation of organotypic hippocampal slice cultures: interface method. Nat Prot 1:1439–1445

43. Gogolla N, Galimberti I, DePaola V et al (2006) Preparation of organotypic hippocampal slice cultures for long-term live imaging. Nat Prot 1:1165–1171

44. Opitz-Araya X, Barria A (2011) Organotypic hippocampal slice cultures. J Vis Exp. https://doi.org/10.3791/2462

45. Woods G, Zito K (2008) Preparation of gene gun bullets and biolistic transfection of neurons in slice culture. J Vis Exp. https://doi.org/10.3791/675

46. Harvey CD, Svoboda K (2007) Locally dynamic synaptic learning rules in pyramidal neuron dendrites. Nature 450:1195–1200

47. Lein PJ, Barnhart CD, Pessah IN (2011) Acute hippocampal slice preparation and hippocampal slice cultures. Methods Mol Biol 758:115–134

48. Feng G, Mellor RH, Bernstein M et al (2000) Imaging neuronal subsets in transgenic mice expressing multiple spectral variants of GFP. Neuron 28:41–51

49. Sjulson L, Cassataro D, DasGupta S et al (2016) Cell-specific targeting of genetically encoded tools for neuroscience. Annu Rev Genet 50:571–594

50. Tabata H, Nakajima K (2001) Efficient in utero gene transfer system to the developing mouse brain using electroporation: visualization of neuronal migration in the developing cortex. Neuroscience 103:865–872

51. Bedbrook CN, Deverman BE, Gradinaru V (2018) Viral strategies for targeting the central and peripheral nervous systems. Annu Rev Neurosci 41:323–348

52. Eilers J, Konnerth A (2009) Dye loading with patch pipettes. Cold Spring Harb Protoc 2009:pdb prot5201

53. Nevian T, Helmchen F (2007) Calcium indicator loading of neurons using single-cell electroporation. Pflugers Arch 454:675–688

54. Svoboda K, Yasuda R (2006) Principles of two-photon excitation microscopy and its applications to neuroscience. Neuron 50:823–839

55. Suter BA, O'Connor T, Iyer V et al (2010) Ephus: multipurpose data acquisition software for neuroscience experiments. Front Neural Circuits. https://doi.org/10.3389/fncir.2010.00100

56. Raghavachari S, Lisman JE (2004) Properties of quantal transmission at CA1 synapses. J Neurophysiol 92:2456–2467

57. Bloodgood BL, Sabatini BL (2007) Nonlinear regulation of unitary synaptic signals by CaV(2.3) voltage-sensitive calcium channels located in dendritic spines. Neuron 53:249–260

58. Zhang YP, Holbro N, Oertner TG (2008) Optical induction of plasticity at single synapses reveals input-specific accumulation of αCaMKII. Proc Natl Acad Sci U S A 105:12039–12044

59. Oh WC, Parajuli LK, Zito K (2015) Heterosynaptic structural plasticity on local dendritic segments of hippocampal CA1 neurons. Cell Rep 10:162–169

60. Bosch M, Castro J, Saneyoshi T et al (2014) Structural and molecular remodeling of dendritic spine substructures during long-term potentiation. Neuron 82:444–459

61. Lee SJ, Escobedo-Lozoya Y, Szatmari EM et al (2009) Activation of CaMKII in single dendritic spines during long-term potentiation. Nature 458:299–304

62. Kato K, Clifford DB, Zorumski CF (1993) Long-term potentiation during whole-cell recording in rat hippocampal slices. Neuroscience 53:39–47

63. Malinow R, Tsien RW (1990) Presynaptic enhancement shown by whole-cell recordings of long-term potentiation in hippocampal slices. Nature 346:177–180

64. Holtmaat AJ, Trachtenberg JT, Wilbrecht L et al (2005) Transient and persistent dendritic spines in the neocortex in vivo. Neuron 45:279–291

65. Hedrick NG, Yasuda R (2017) Regulation of Rho GTPase proteins during spine structural plasticity for the control of local dendritic plasticity. Curr Opin Neurobiol 45:193–201

66. Murakoshi H, Wang H, Yasuda R (2011) Local, persistent activation of Rho GTPases during plasticity of single dendritic spines. Nature 472:100–104

67. Zhai S, Ark ED, Parra-Bueno P et al (2013) Long-distance integration of nuclear ERK signaling triggered by activation of a few dendritic spines. Science 342:1107–1111